Hindawi
Shock and Vibration
Volume 2020, Article ID 2606178, 10 pages
https://doi.org/10.1155/2020/2606178

Research Article

Unbalance Suppression for AMB Rotor System Using APF-SRF Algorithm

Yuanping Xu,[1] **Haitong Wu**,[2] **and Xudong Guan**[2]

[1]*National Key Laboratory of Science and Technology on Helicopter Transmission, Nanjing University of Aeronautics and Astronautics, Nanjing 210016, China*
[2]*College of Mechanical and Electrical Engineering, Nanjing University of Aeronautics and Astronautics, Nanjing 210016, China*

Correspondence should be addressed to Yuanping Xu; ypxu@nuaa.edu.cn

Received 28 July 2019; Revised 18 December 2019; Accepted 24 December 2019; Published 20 January 2020

Academic Editor: Marco Tarabini

With the great capability in levitating rotors, active magnetic bearings (AMB) have been increasingly applied in high-speed rotating machinery applications. Typically, for the practical application of AMB rotor systems, synchronous unbalance vibration has long been a critical issue. Thus, exploring a facile yet effective approach to address this issue has attracted tremendous interest from both industrial and academic perspectives. Herein, in this work, we propose a novel strategy to suppress the unbalance vibration through a compensation control algorithm method. The compensation control algorithm which is established based on the combination of first-order all-pass filter (APF) and synchronous rotating frame (SRF) algorithm demonstrates to be efficient in greatly reducing the unbalance vibration and resulting in excellent system stability according to both simulation and experimental results. This work not only confirms the applicability of APF-SRF algorithm for the AMB rotor systems but also opens up a new paradigm to modulate and minimize the unbalance vibration of AMB rotor systems.

1. Introduction

With the main function of reducing friction between moving parts, bearing acts as one of the most important components in rotating machinery. Among the various bearings such as conventional ball and air and sliding bearings, active magnetic bearings possess the inherent merits of avoiding mechanical frictions and eliminating lubrication, which make them highly desirable for constructing high-speed rotating machinery including blower, compressor, bearingless motor, and turbomachinery [1–6].

However, for the practical application of AMB rotor systems, the synchronous unbalance vibration phenomenon has long been a critical issue. Typically, the unbalance vibration induced by the mass unbalance of rotor would deteriorate the stabilization of the bearings system and cause serious damage effect. Thus, exploring an effective approach to suppress the unbalance vibration of AMB rotor systems has triggered enormous interest from both academic and industrial communities.

To date, in the last three decades, a large number of unbalance vibration suppression control techniques have been developed. For instance, Herzog et al. [7] presented a generalized narrow-band notch filter for the AMB rotor system and provided industrial unbalance compensation application results. Zhu et al. [8, 9] proposed the iterative seeking algorithm to produce additional forces to reduce the rotor vibration which is suitable for both fix speed and varying speed conditions. Lum et al. [10] presented an adaptive auto-centering unbalance compensation method, which is frequency independent and suitable for varying speed conditions. Based on the filtered-x LMS adaptive filter, Shi et al. [11] proposed an adaptive feedforward unbalance suppression algorithm for AMB rotor systems with unknown mass imbalance. Cui et al. [12] proposed an improved robust odd repetitive control method to suppress the periodic vibration. Peng et al. [13] developed a multiple resonant control strategy for AMB rotor systems to suppress the multifrequency current harmonics during the varying speed conditions. Chen et al. [14] designed a fuzzy PID

controller, thus reducing the unbalance vibration. Chen et al. [15] applied the adaptive immersion and invariance control method to compensate the unbalance force for a strong nonlinearity three-pole AMB system. Noshadi and Zolfagharian [16] demonstrated an unbalance suppression method through varying speed conditions by introducing an inner-loop repetitive disturbance observer-based controller.

Typically, the reported various techniques including these mentioned above can be mainly classified into two categories according to the different mechanisms. The basic mechanism for the first category is to provide magnetic bearings with higher magnetic control stiffness to force the rotor spin around its axis of geometry compulsorily [17, 18]. This strategy proves to be applicable for those situations requiring high rotating precision, i.e., spindle. However, on the other hand, using this approach may give rise to the saturation of power amplifier. The core mechanism of the second category lies in making the rotor to rotate around its inertial axis to reduce unbalance vibration [7, 19]. Moreover, there are also further unbalance control strategies to improve the system stability while passing bending critical speeds [20].

In this work, we present a novel approach based on the combination of first-order all-pass filter (APF) and synchronous rotating frame (SRF) algorithm to minimize the unbalance vibration of AMB rotor systems. For the first time, the SRF method which has been widely adopted in electric and electronic systems [21–25] was applied in the AMB rotor system for unbalance compensation [26]. Making use of the SRF-based method, one can realize the good stability of AMB rotor systems by only adjusting the compensate angle. It also should be pointed out here that according to the hypothesis of previous work, the rotor displacement measurements in the two orthogonal axes possess the same amplitude with a phase difference of $\pi/2$. However, in the real AMB rotor system, even though we can use the same control parameters to improve the isotropy, the anisotropy for x and y direction is still inevitable and thus the rotor displacement orbit is not always an ideal circle (see Figure 1) due to the discrepancy in manufacturing process and electrical component performance. Such phenomenon may greatly limit the SRF-based controller performance. Herein, to address this problem, we propose a more practical algorithm for AMB rotor unbalance compensation. The principle of APF-SRF algorithm is given, and the stability analysis of the AMB rotor system using this proposed APF-SRF algorithm is performed. Both simulation and experimental results confirm the efficiency of this novel APF-SRF algorithm in suppressing unbalance vibration of the AMB rotor system and meanwhile ensuring its good stability.

The remainder of paper is organized as follows. First, Section 2 describes the principles of the proposed APF-SRF unbalance suppression algorithm. Next, we present the simulation and experimental results in Section 3. Last, conclusions are drawn in Section 4.

2. Principles

2.1. SRF Algorithm. The SRF algorithm is usually adopted to extract the harmonics by using Park transformation, which

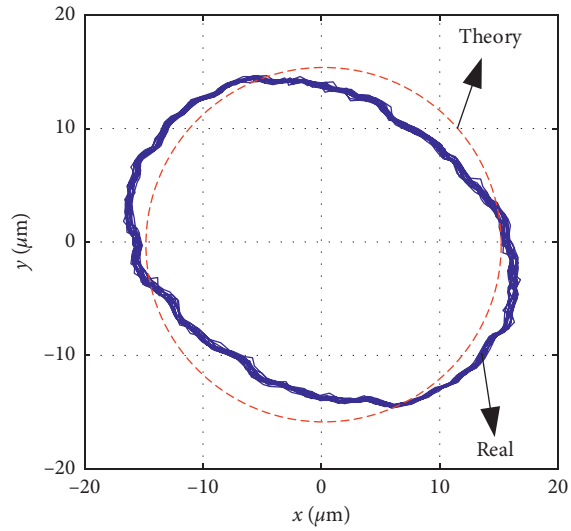

Figure 1: Rotor displacement orbit due to the performance discrepancy in x and y directions.

is also known as the d-q method [22, 27]. The Park transformation matrix is described as follows:

$$T(\omega t) = \begin{bmatrix} \cos(\omega t) & \sin(\omega t) \\ -\sin(\omega t) & \cos(\omega t) \end{bmatrix}. \tag{1}$$

The block diagram of the SRF algorithm is pictured in Figure 2. The $[x_\alpha, x_\beta]$ denote the two orthogonal periodic discrete-time signals which have the same amplitude and frequency in a stationary frame. Therefore, using the discrete Fourier series, they can be written as follows:

$$\begin{bmatrix} x_\alpha \\ x_\beta \end{bmatrix} = \begin{bmatrix} \sum_{n=1}^{\infty} A_n \cos(n\omega t + \theta_n) \\ \sum_{n=1}^{\infty} A_n \sin(n\omega t + \theta_n) \end{bmatrix}. \tag{2}$$

Using Park transformation, (3) could be obtained by multiplying (1) with (2) and simplified using the trigonometric formula as follows:

$$\begin{bmatrix} x_d \\ x_q \end{bmatrix} = T(\omega t) \begin{bmatrix} x_\alpha \\ x_\beta \end{bmatrix} = \begin{bmatrix} \sum_{n=1}^{\infty} A_n \cos[(n-1)\omega t + \theta_n] \\ \sum_{n=1}^{\infty} A_n \sin[(n-1)\omega t + \theta_n] \end{bmatrix}, \tag{3}$$

where x_d and x_q are the outputs of the Park transformation in the synchronous frame. From (3), it is clear that after being transformed by the Park transformation, the fundamental and harmonics components can be separated easily. For the AMB rotor system, the high-frequency harmonic components will induce high-frequency vibration, which can be filtered out by applying a low-pass filer (LPF), and the fundamental components can be described as follows:

$$\begin{bmatrix} x_d \\ x_q \end{bmatrix} = \begin{bmatrix} A_1 \cos\theta_1 \\ A_1 \sin\theta_1 \end{bmatrix}. \tag{4}$$

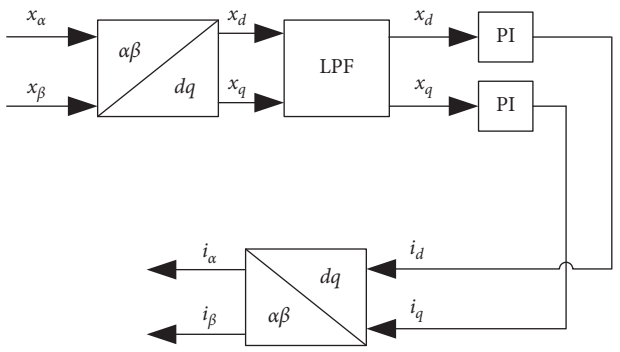

Figure 2: SRF algorithm block diagram.

The filtered outputs of the Park transformation are compared with their references values, and the PI controller is employed to avoid steady state error. The PI controller has an infinite gain for the DC component. When the system reaches the steady state, the gain of the PI controller could be denoted as K. Thus, we can obtain the equation described as follows:

$$\begin{bmatrix} i_d \\ i_q \end{bmatrix} = \begin{bmatrix} KA_1 \cos\theta_1 \\ KA_1 \sin\theta_1 \end{bmatrix}. \tag{5}$$

Finally, using the inverse Park transformation, the stationary frame fundamental component at ω can be obtained as follows:

$$\begin{bmatrix} i_\alpha \\ i_\beta \end{bmatrix} = T_{\text{inv}}(\omega t) \begin{bmatrix} i_d \\ i_q \end{bmatrix}, \tag{6}$$

where

$$T_{\text{inv}}(\omega t) = \begin{pmatrix} \cos(\omega t + \varphi) & -\sin(\omega t + \varphi) \\ \sin(\omega t + \varphi) & \cos(\omega t + \varphi) \end{pmatrix}, \tag{7}$$

where φ represents the compensation phase angle and can be used to ensure the close-loop system stability. Therefore, (6) can be written as

$$\begin{bmatrix} i_\alpha \\ i_\beta \end{bmatrix} = \begin{bmatrix} KA_1 \cos(\omega t + \theta_1 + \varphi) \\ KA_1 \sin(\omega t + \theta_1 + \varphi) \end{bmatrix}. \tag{8}$$

From (8), it is clear that the control signals i_α and i_β have the same frequency, but with a phase lead φ.

2.2. First-Order All-Pass Filter. As described above, the transformation from the stationary frame to the synchronous frame using Park transformation requires two orthogonal components which possess the same amplitude and frequency. However, in the real AMB rotor system, the discrepancy in manufacturing process and electrical components performance would result in the anisotropy in x and y directions, giving rise to limited SRF-based controller performance. To overcome the limitation, the first-order all-pass filter (APF) is employed in this work to generate two quadrature signals. APF is widely applied in the signal processing, and it could shift the phase of an input signal from 0 to π while keeping the amplitude constant. Consequently, it can be used in the instrumentation and communication systems such as multiphase oscillators [28–30]. The first-order APF transfer function is given by

$$G_{\text{APF}}(s) = \frac{\omega_0 - s}{\omega_0 + s}, \tag{9}$$

where ω_0 represents the corner frequency of the system of the first-order APF. This transfer function has unity gain for all frequencies and a phase lag:

$$\phi = -2\arctan\left(\frac{\omega}{\omega_0}\right), \tag{10}$$

where phase lag ϕ varies from 0 to −180 degrees as ω goes from zero to infinity. Bode plots from transfer function of (10) are shown in Figure 3. It can be concluded from Figure 3 that the shifting phase is zero while ω is DC and −90 degree when $\omega = \omega_0$. Therefore, for the input signal with frequency of ω_0, the first-order APF can shift its phase with 90 degrees. If the ω_0 is a variable and equals to the rotor displacement synchronous component, the first-order APF output is always 90 degrees lagged from input rotor displacement signal. Therefore, one axis rotor displacement signal could generate two quadrature signals, which will satisfy the SRF algorithm requirement.

2.3. APF-SRF Unbalance Suppression. Combining the first-order APF and SRF together, the closed-loop AMB rotor system control block diagram involving the APF-SRF unbalance suppression controller is shown in Figure 4. Here, $H(s)$ is the unbalance suppression controller, $C(s)$ is the original levitation controller, $A(s)$ represents the amplifier, $P(s)$ represents the controlled plant, and K_s denotes the displacement sensor.

The unbalance suppression controller $H(s)$ is connected in parallel with the original system levitation controller $C(s)$, and the detected displacement deviation is the input. The unbalance suppression signals are added to the original system controller output. Figure 5 gives the specific structure of unbalance suppression controller $H(s)$, which contains a first-order APF and a SRF. The rotor displacement signal x is transformed to two signals $[x_\alpha, x_\beta]$, which have the same amplitude but 90 degrees lagged using first-order APF. Then, the two signals $[x_\alpha, x_\beta]$ are transformed to DC component $[x_d, x_q]$ with Park transformation. For the rotor bearings system, considering the periodic forced excitation with frequency ω, the unbalance response is typical with the frequency of excitation coinciding with rotor speed, i.e., $\omega = \Omega$. Therefore, the ω could be obtained from the speed sensor. To filter the high-frequency components, a first-order low-pass filter is employed in this work and its transfer function is

$$G_f(s) = \frac{1}{\tau s + 1}, \tag{11}$$

where $\tau = 1/(2\pi f_c)$ and, in this paper, $f_c = 10$ Hz. Then, the PI controller guarantees no steady state error for the filtered signals and the PI controller transfer function is

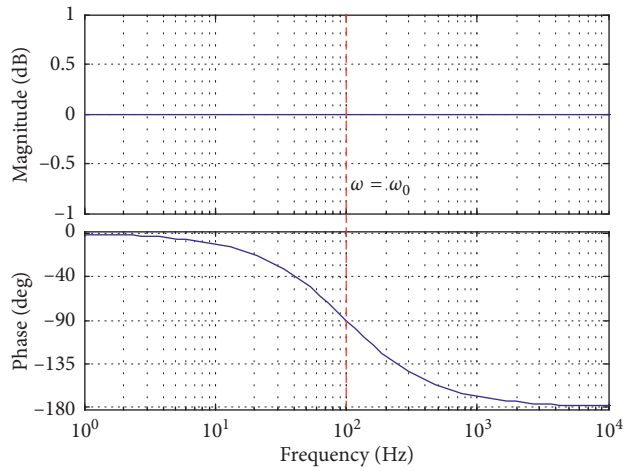

Figure 3: Bode plot of first-order APF.

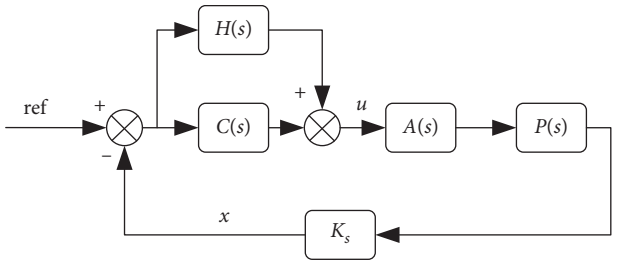

Figure 4: Block diagram of the closed-loop control system involving the APF-SRF unbalance suppression controller.

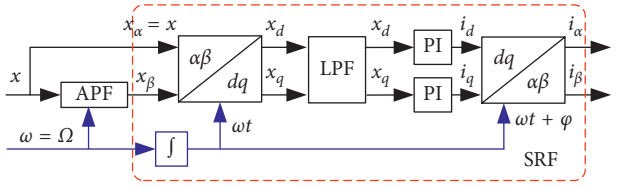

Figure 5: Structure of the APF-SRF unbalance suppression controller.

$$G_{\mathrm{PI}}(s) = k_p + \frac{k_i}{s}, \tag{12}$$

where k_p is the proportional coefficient and k_i is the integral coefficient. In this paper, $k_p = 0.5$ and $k_i = 3$. The PI controller output signals $[i_d, i_q]$ are transformed to control signals $[i_\alpha, i_\beta]$ by applying the inverse Park transformation, and these control signals are added to the original system controller to suppress the same frequency vibration.

2.4. Stability Analysis. The transfer function of the first-order low-pass filter and PI controller in the stationary frame can be analyzed in the frequency domain [26] to obtain

$$\begin{aligned}\widehat{G}_f(s)\widehat{G}_{PI}(s) &= G_f(s - j\omega)G_{\mathrm{PI}}(s - j\omega)e^{j\varphi} \\ &= \frac{1}{\tau(s - j\omega) + 1}\left(k_p + \frac{k_i}{s - j\omega}\right)e^{j\varphi}.\end{aligned} \tag{13}$$

Thus, the transfer function of APF-SRF unbalance suppression controller can be written as

$$H(s) = \frac{i_\alpha}{x} = \frac{\left(k_p(s - j\omega) + k_i\right)e^{j\varphi}}{(\tau(s - j\omega) + 1)(s - j\omega)}. \tag{14}$$

Therefore, as shown in Figure 4, the characteristic equation of the closed-loop system is

$$1 + (C(s) + H(s))A(s)P(s)K_s = 0. \tag{15}$$

(15) can be rewritten as

$$1 + \frac{H(s)A(s)P(s)K_s}{1 + C(s)A(s)P(s)K_s} = 0. \tag{16}$$

As shown in Figure 4, without unbalance suppression controller $H(s)$, the closed-loop transfer function from amplifier input u to sensor output x could be written as

$$R(s) = \frac{A(s)P(s)K_s}{1 + C(s)A(s)P(s)K_s}. \tag{17}$$

Therefore, substituting (14) and (17) into (16) yields

$$\begin{aligned}\varsigma(s, k_i) &= (s - j\omega)\left[(\tau(s - j\omega) + 1) + k_p e^{j\varphi}R(s)\right] \\ &\quad + k_i e^{j\varphi}R(s) = 0.\end{aligned} \tag{18}$$

The derivative of (18) with respect to k_i can be obtained when $k_i = 0$ is as follows:

$$\begin{aligned}\left.\frac{\partial s(k_i)}{\partial k_i}\right|_{s=j\omega, k_i=0} &= -\frac{\partial\varsigma(s, k_i)/\partial k_i}{\partial\varsigma(s, k_i)/\partial s} \\ &= -\frac{e^{j\varphi}R(j\omega)}{1 + k_p e^{j\varphi}R(j\omega)}.\end{aligned} \tag{19}$$

The AMB rotor system is stable before the APF-SRF is added; therefore, $R(s)$ is stable. After plunging the APF-SRF controller, in order to satisfy the stability requirements to ensure the motion of root locus to left, we can conclude from (19) that

$$\begin{cases}\mathrm{Re}\left[-\dfrac{e^{j\varphi}R(j\omega)}{1 + k_p e^{j\varphi}R(j\omega)}\right] < 0, \\ \mathrm{Im}\left[-\dfrac{e^{j\varphi}R(j\omega)}{1 + k_p e^{j\varphi}R(j\omega)}\right] = 0.\end{cases} \tag{20}$$

The stability condition of (20) is equivalent to the following:

$$-\frac{\pi}{2} < \arg\left(-\frac{e^{j\varphi}R(j\omega)}{1 + k_p e^{j\varphi}R(j\omega)}\right) < \frac{\pi}{2}. \tag{21}$$

From (21), we can conclude that the system stability is related to the PI parameters, the compensation phase angle φ, and $R(s)$. With the appropriate PI parameters, the stability of the closed-loop system can be guaranteed by tuning the complement phase angle.

3. Simulation and Experimental Results

3.1. Experimental System. Figure 6 shows the mechanical structure of the experiential AMB rotor employed in this

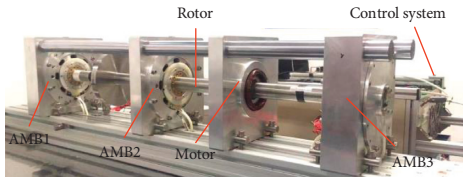

Figure 6: Structure of the AMB rotor.

work. The length of the rotor is around 1m, and the weight is around 14.5 kg. Three AMB (AMB1, AMB2, and AMB3) are assembled in this test rig, and in this work, only AMB1 and AMB3 are activated for rotor levitation. Another radial AMB located around the center of the rotor (AMB2) is designed as the noncontact electromagnetic exciter to apply online electromagnetic force during the operation. A 5 kW induction motor provides rotating power for the rotor. The air gaps for radial and thrust AMB are 0.25 mm and 0.6 mm, respectively. Table 1 lists the other parameters of the test rig. Figure 7 presents the radial and thrust AMB adopted in this work.

The rotor is modeled using the finite element method and Nelson–Timoshenko beam is adopted. The rotor is split into 69 elements, and Figure 8 shows the theoretical free-free undamped mode shapes of the rotor. Considering the bearing stiffness and gyroscopic effect, a Campbell diagram is drawn at 10^6 N/m support stiffness, as illustrated in Figure 9. With the gyroscopic effects, the natural frequencies are the functions of the rotor speed and splitting into forward and backward modes.

The control program is implemented on a dSPACE1202 MicroLabBox, and the sample rate was set as 20 kHz. The decentralized PID control strategy is employed to stabilize the AMB rotor system, and its PID coefficients are $k_{pc} = 1.7$, $k_{ic} = 1$, and $k_{dc} = 0.003$. The whole system is pictured in Figure 10.

3.2. Simulation. For the AMB rotor system, the system is open-loop unstable and the feedback closed-loop control is indispensable due to the magnetic force property. Therefore, stability is the primary concern for the AMB rotor system. Using the system parameters mentioned above, Figure 11 presents the closed-loop system-dominant root locus in the complex plane depending on the phase compensation angle φ. It is clear that without phase compensation ($\varphi = 0$), the root loci (red color) move to the right direction with increasing speed. At the speed of 35 Hz, the root loci cross the image axis and then enter the right-half plane with increasing rotating speed. The root loci located at the right-half plane mean that the system loses stability with the proposed unbalance compensation method when $\varphi = 0$. To stabilize the system, phase-frequency characteristic of the $R(s)$ function is adopted as phase compensation angle and the blue dot is the root loci with introducing the phase compensation angle. It is clear that the root loci locate at the entire left-half plane over the operation speed range indicating the system remains stable.

Table 1: Basic parameters of the test rig.

Symbol	Quantity	Values
m	Rotor mass	14.5 kg
K_i	Force/current factor	91.5 N/A
K_x	Force/displacement factor	7.3×10^5 N/m
K_{amp}	Amplifier gain	0.4 A/V
f_w	Amplifier cutoff frequency	1224 Hz
K_s	Sensor gain	20000 V/m

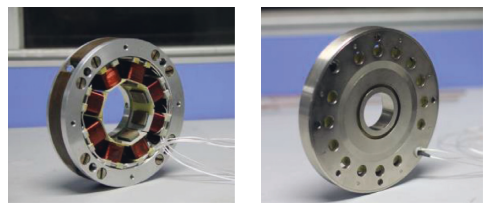

(a) (b)

Figure 7: The radial and thrust AMB employed in this paper. (a) Radial AMB. (b) Thrust AMB.

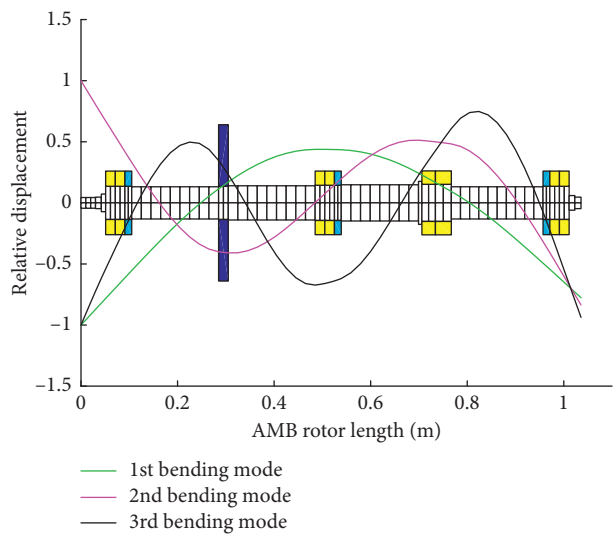

Figure 8: Theoretical free-free mode shapes of the rotor.

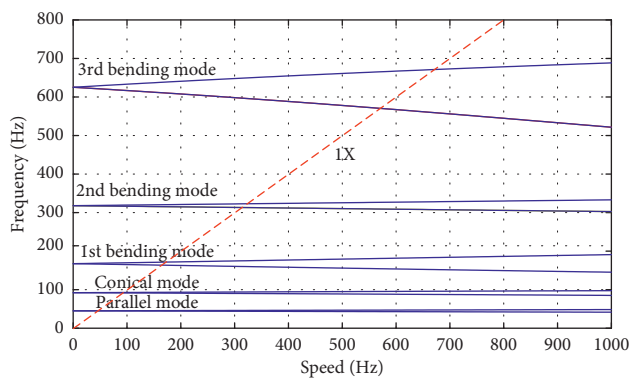

Figure 9: Campbell diagram showing splitting of natural frequencies at 10^6 N/m support stiffness.

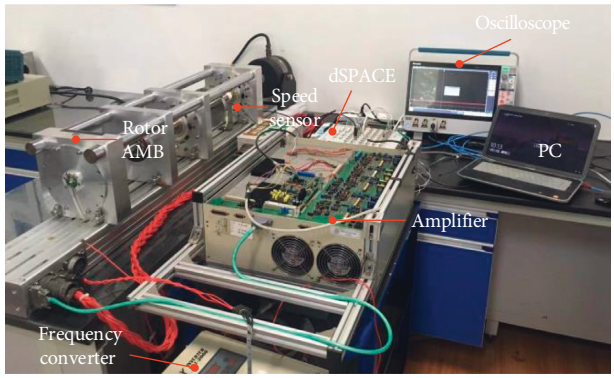

Figure 10: AMB rotor system.

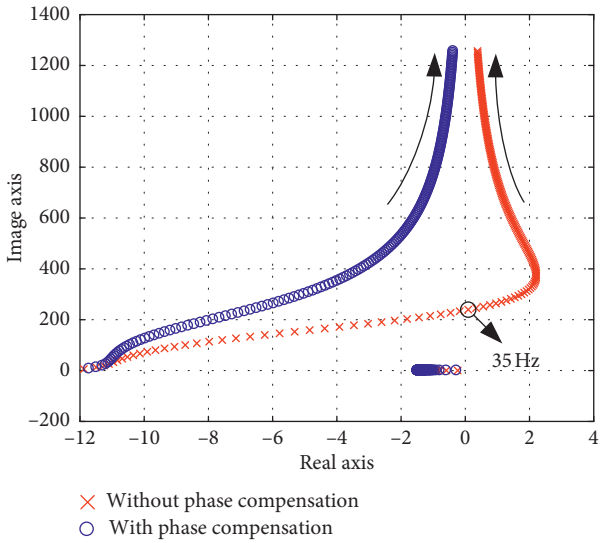

Figure 11: Closed-loop-dominant root locus.

To simulate the system performance, the rotor unbalance response is calculated. From $t = 0$ s to $t = 0.5$ s, the APF-SRF unbalance suppression controller is disabled. Two phase compensation situation, $\varphi = 0$ and $\varphi = \pi/2$ are tested. Figure 12(a) shows the simulated displacement vibration at 35 Hz with $\varphi = 0$. When the unbalance suppression controller is activated, the displacement vibration becomes divergence and the filtered DC output becomes unstable (Figure 12(b)), which means the AMB rotor system is out of control. Figure 12(c) shows the simulated displacement vibration at 35 Hz with $\varphi = \pi/2$. When the unbalance suppression controller is activated, the displacement vibration can be minimized and the filtered DC output is convergent, as indicated in Figure 12(d).

The simulation results indicate that with the appropriate compensation phase angle φ to ensure the system stability, the APF-SRF algorithm is an effective method for AMB rotor system unbalance suppression.

3.3. Experimental Results. The control program is implemented on a dSPACE1202 MicroLabBox, and the sample rate was set as 20 kHz. The decentralized PID control

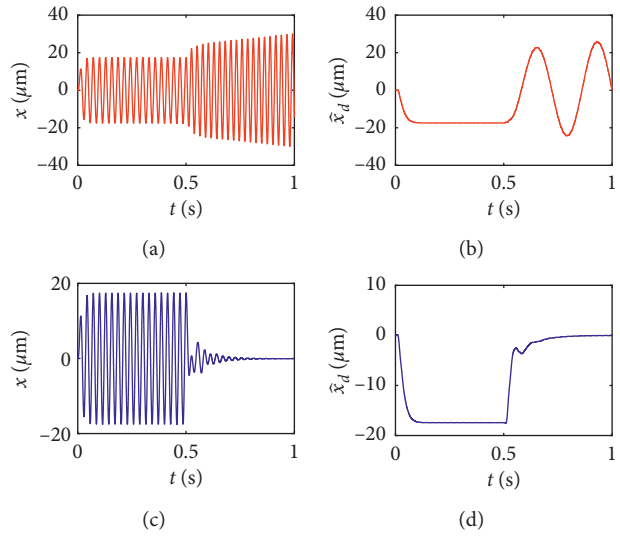

Figure 12: Simulation results of the AMB rotor system using APF-SRF unbalance compensation algorithm. (a) Rotor displacement with $\varphi = 0$. (b) Filtered output with $\varphi = 0$. (c) Rotor displacement with $\varphi = \pi/2$. (d) Filtered output with $\varphi = \pi/2$.

strategy is employed to stabilize the AMB rotor system. In the test, the phase compensation angle is acquired from the transfer function $R(s)$ using the sine sweeping test from the real test rig in the levitation condition.

Firstly, a fixed rotating speed 9000 rpm is selected to evaluate the proposed APF-SRF unbalance compensation algorithm. Figure 13 shows the changes of rotor displacement at 9000 rpm while the proposed unbalance suppression method is activated. The maximum displacement amplitudes for both AMB1 and AMB3 in two orthogonal directions are almost suppressed from 15 μm to 5 μm. Figure 14 shows the comparison of rotor displacement orbits at 9000 rpm for both AMB1 and AMB3 with an unbalance compensation controller or not, for which the same conclusions can be obtained.

To evaluate the proposed method in the variable speed condition, the rotor was decelerated from 11100 to 0 rpm with the proposed unbalance compensation algorithm. Figure 15 gives the displacement amplitude from 11100 to 0 rpm using the proposed unbalance compensation algorithm. For the sake of comparison, the corresponding displacement amplitude with the absence of proposed unbalance compensation algorithm is also given, as illustrated in Figure 16. Obviously, the proposed method demonstrates to be effective in suppressing the unbalance phenomenon and stablizing the system, particularly at high speed. It also should be noted here that due to the different vibration conditions, the deceleration time of the two figures exists as a weak discrepancy.

The ISO14839-2:2004 (vibration of rotating machinery equipped with active magnetic bearings-part 2: evaluation of vibration) standard is selected for evaluation. According to ISO14839-2:2004, the vibration index is defined $D_{\max}/C_{\min}$, where $D_{\max}$ is the maximum peak displacement which is

$$D_{\max} = \max\left[\sqrt{x^2(t) + y^2(t)}\right], \tag{22}$$

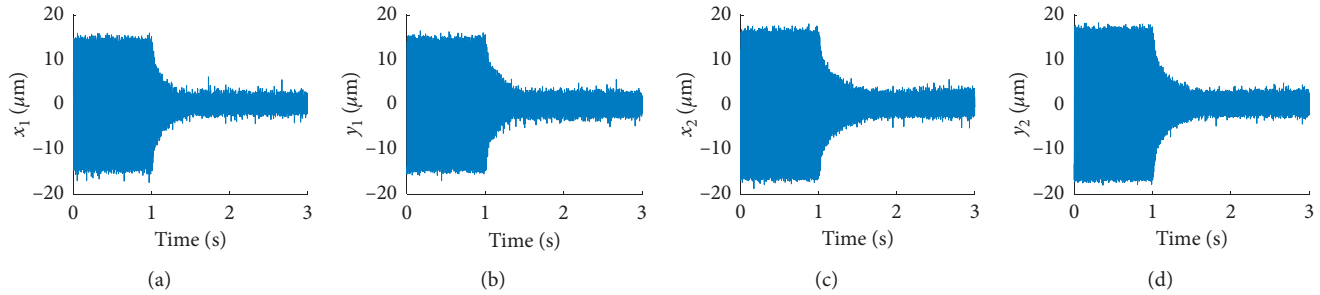

FIGURE 13: The changes of rotor displacement at 9000 rpm with the proposed APF-SRF unbalance compensation algorithm. (a) AMB1 x direction. (b) AMB1 y direction. (c) AMB3 x direction. (d) AMB3 y direction.

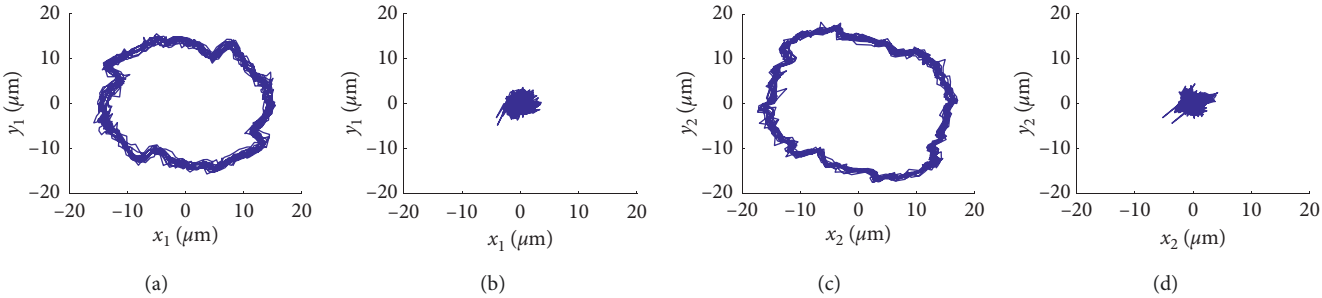

FIGURE 14: Rotor displacement orbits at 9000 rpm. (a) AMB1 without unbalance compensation. (b) AMB1 with unbalance compensation. (c) AMB3 without unbalance compensation. (d) AMB3 with unbalance compensation.

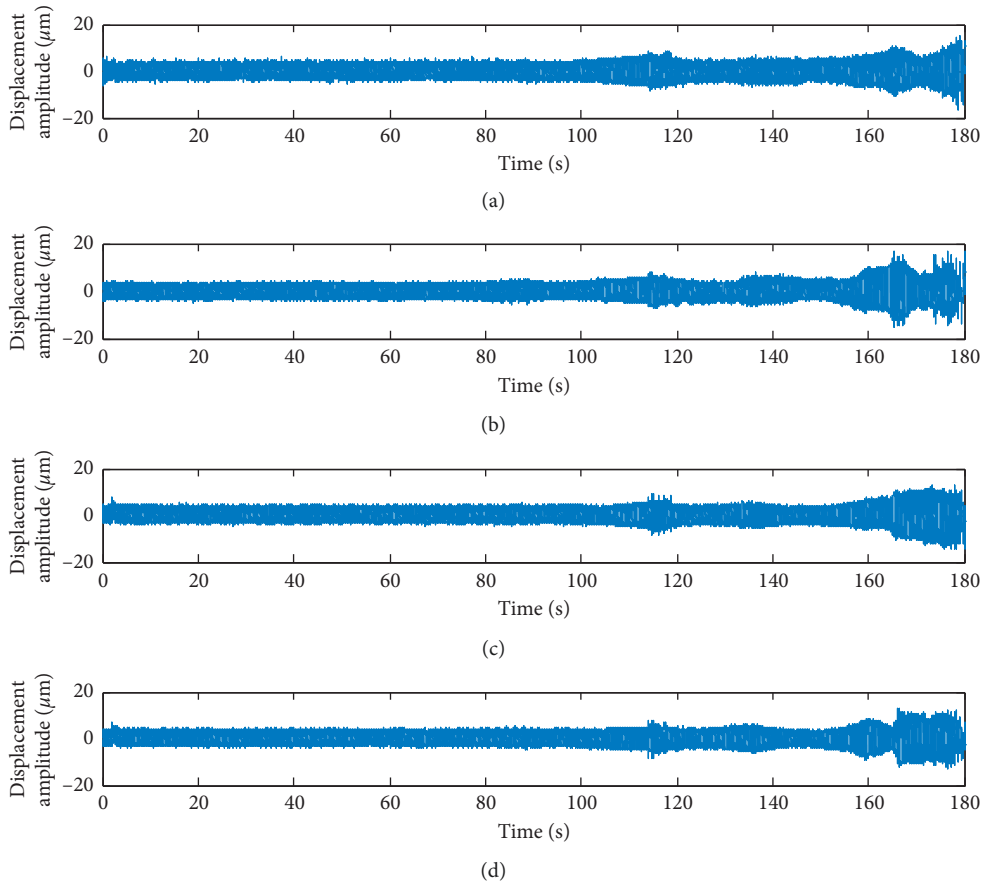

FIGURE 15: Displacement amplitude from11100 to 0 rpm using the proposed unbalance compensation algorithm. (a) AMB1 x direction. (b) AMB1 y direction. (c) AMB3 x direction. (d) AMB3 y direction.

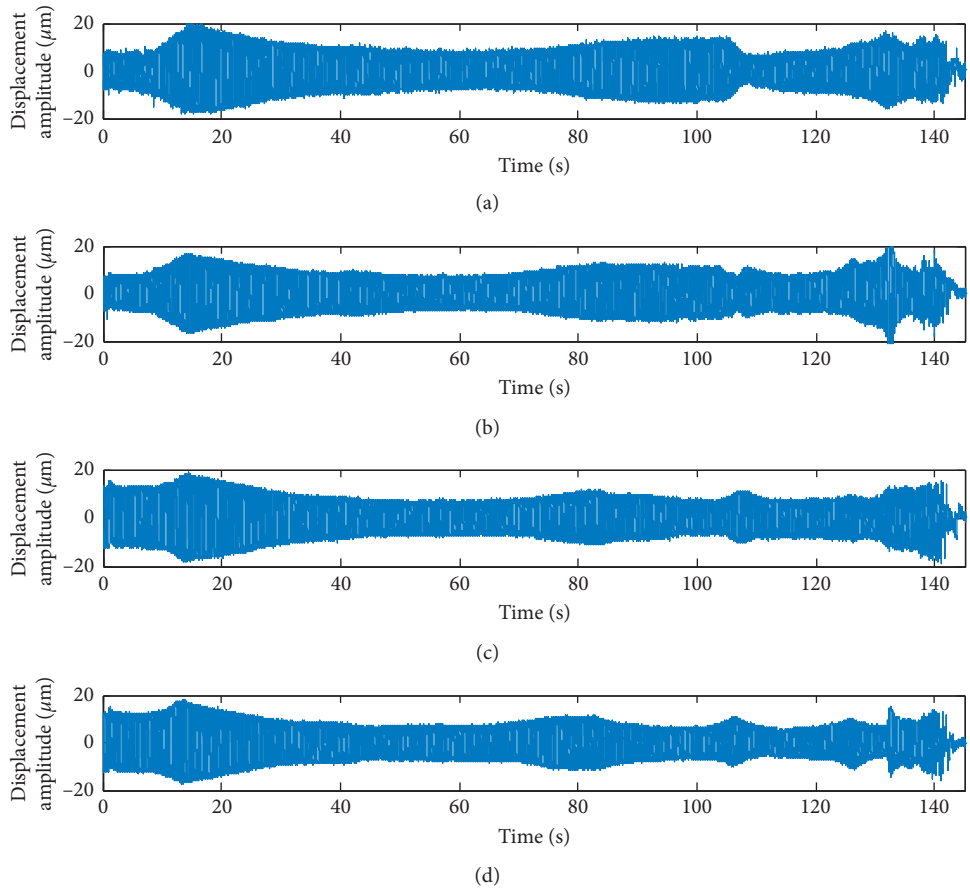

Figure 16: Displacement amplitude from11100 to 0 rpm with the absence of proposed unbalance compensation algorithm. (a) AMB1 x direction. (b) AMB1 y direction. (c) AMB3 x direction. (d) AMB3 y direction.

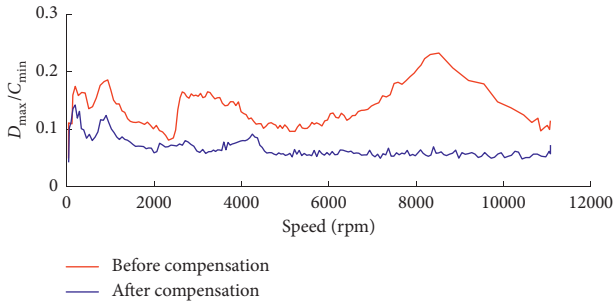

Figure 17: The comparison of the vibration index for AMB1.

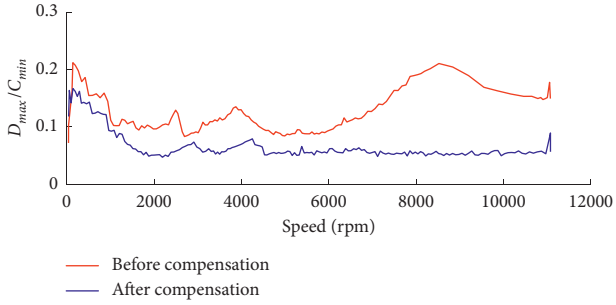

Figure 18: The comparison of the vibration index for AMB3.

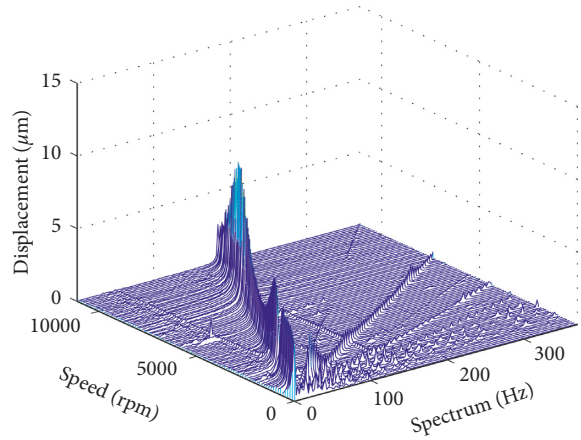

Figure 19: Comparison rotor displacement waterfall diagram in AMB1 x direction without algorithm.

where C_{min} is the minimum value of radial or axial clearance between the rotor and stator. Figure 17 shows the comparison of the vibration index for AMB1 depending on with the proposed method or without. In the entire speed range, the proposed method could stabilize the system and possess well unbalance suppressionperformance. Figure 18 shows the comparison of the vibration index for AMB3, and we can obtain the same conclusion.

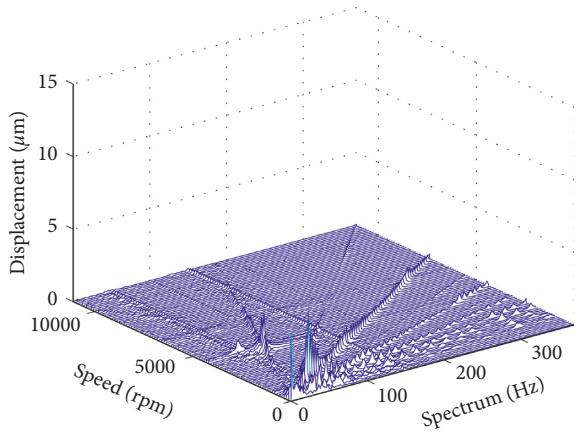

Figure 20: Comparison rotor displacement waterfall diagram in AMB1 x direction with APF-SRF unbalance compensation algorithm.

Figure 19 shows the rotor displacement waterfall diagram in AMB1 x direction without any suppression method over the entire speed range. We can find that a maximum synchronous displacement vibration is up to 9.3 μm at 8340 rpm. Figure 20 shows the rotor displacement waterfall diagram in AMB1 x direction with the proposed suppression method over the entire speed range, and it is clear that the proposed method is very effective especially at high speed.

4. Conclusion

Synchronous unbalance vibration has long been a critical issue for the practical application of AMB. In this work, we propose a feedforward compensation controller to suppress the unbalance vibration, which is rooting in the combination of APF and SRF transformation. The proposed algorithm demonstrates to be more effective over the traditional SRF-based control method by generating two orthogonal components using APF. Simply applying the APF-SRF algorithm to the AMB rotor system may lead to instability, and a compensation phase angle is introduced further to ensure a good stability. According to both simulation and experimental results, the APF-SRF algorithm proves to be efficient in suppressing unbalance vibration of AMB rotor system, meanwhile ensuring its good stability. This work not only demonstrates the applicability of APF-SRF algorithm for the AMB rotor system but also opens up a new paradigm to modulate and minimize the unbalance vibration of the AMB rotor system.

Data Availability

The experimental figure data used to support the findings of this study are included within the article. The Matlab simulation, control program data used to support the findings of this study are available from the corresponding author.

Conflicts of Interest

The authors declare that there are no conflicts of interest regarding the publication of this paper.

Acknowledgments

This work was supported in part by the National Natural Science Foundation of China (51905263), Key Laboratory of Vibration and Control of Aero-Propulsion System, Ministry of Education (VCAME201902), Jiangsu Natural Science Youth Fund (BK20190412), China Postdoctoral Science Foundation (2018M642245), Jiangsu Postdoctoral Research Funding (2019K188), and Fundamental Research Funds for the Central Universities (NZ2018460).

References

[1] E. H. Maslen and G. Schweitzer, *Magnetic Bearings*, Springer, Berlin, Germany, 2009.

[2] A. H. Pesch, A. Smirnov, O. Pyrhonen, and J. T. Sawicki, "Magnetic bearing spindle tool tracking through," *IEEE/ASME Transactions on Mechatronics*, vol. 20, no. 3, pp. 1448–1457, 2015.

[3] S. Zheng, B. Han, Y. Wang, and J. Zhou, "Optimization of damping compensation for a flexible rotor system with active magnetic bearing considering gyroscopic effect," *IEEE/ASME Transactions on Mechatronics*, vol. 20, no. 3, pp. 1130–1137, 2015.

[4] T. M. Lim and S. Cheng, "Parameter estimation and statistical analysis on frequency-dependent active control forces," *Mechanical Systems and Signal Processing*, vol. 21, no. 5, pp. 2112–2124, 2007.

[5] S. E. Mushi, Z. Lin, and P. E. Allaire, "Design, construction, and modeling of a flexible rotor active magnetic bearing test rig," *IEEE/ASME Transactions on Mechatronics*, vol. 17, no. 6, pp. 1170–1182, 2012.

[6] Q. Chen, G. Liu, and B. Han, "Suppression of imbalance vibration in AMB-rotor systems using adaptive frequency estimator," *IEEE Transactions on Industrial Electronics*, vol. 62, no. 12, pp. 7696–7705, 2015.

[7] R. Herzog, P. Buhler, C. Gahler, and R. Larsonneur, "Unbalance compensation using generalized notch filters in the multivariable feedback of magnetic bearings," *IEEE Transactions on Control Systems Technology*, vol. 4, no. 5, pp. 580–586, 1996.

[8] C. Mao and C. Zhu, "Unbalance compensation for active magnetic bearing rotor system using a variable step size real-time iterative seeking algorithm," *IEEE Transactions on Industrial Electronics*, vol. 65, no. 5, pp. 4177–4186, 2018.

[9] K. Jiang, C. Zhu, and L. Chen, "Unbalance compensation by recursive seeking unbalance mass position in active magnetic bearing-rotor system," *IEEE Transactions on Industrial Electronics*, vol. 62, no. 9, pp. 5655–5664, 2015.

[10] K.-Y. Lum, V. T. Coppola, and D. S. Bernstein, "Adaptive autocentering control for an active magnetic bearing supporting a rotor with unknown mass imbalance," *IEEE Transactions on Control Systems Technology*, vol. 4, no. 5, pp. 587–597, 1996.

[11] J. Shi, R. Zmood, and L. J. Qin, "The direct method for adaptive feed-forward vibration control of magnetic bearing systems," in *Proceedings of the 7th International Conference on Control, Automation, Robotics and Vision, 2002 (ICARCV)*, vol. 2, pp. 675–680, Singapore, December 2002.

[12] P. Cui, D. Han, G. Zhang, Z. Liu, and B. Han, "Robust odd repetitive controller for magnetically suspended rotor system," *IEEE Transactions on Industrial Electronics*, vol. 66, no. 3, pp. 2025–2033, 2019.

[13] C. Peng, J. Sun, X. Song, and J. Fang, "Frequency-varying current harmonics for active magnetic bearing via multiple resonant controllers," *IEEE Transactions on Industrial Electronics*, vol. 64, no. 1, pp. 517–526, 2017.

[14] K.-Y. Chen, P.-C. Tung, M.-T. Tsai, and Y.-H. Fan, "A self-tuning fuzzy PID-type controller design for unbalance compensation in an active magnetic bearing," *Expert Systems with Applications*, vol. 36, no. 4, pp. 8560–8570, 2009.

[15] S.-L. Chen, S.-Y. Lin, and C. S. Toh, "Adaptive unbalance compensation for a three-pole active magnetic bearing system," *IEEE Transactions on Industrial Electronics*, vol. 67, no. 3, pp. 2097–2106, 2020.

[16] A. Noshadi and A. Zolfagharian, "Unbalance and harmonic disturbance attenuation of a flexible shaft with active magnetic bearings," *Mechanical Systems and Signal Processing*, vol. 129, pp. 614–628, 2019.

[17] L. Li, T. Shinshi, C. Iijima, X. Zhang, and A. Shimokohbe, "Compensation of rotor imbalance for precision rotation of a planar magnetic bearing rotor," *Precision Engineering*, vol. 27, no. 2, pp. 140–150, 2003.

[18] H. M. N. K. Balini, J. Witte, and C. W. Scherer, "Synthesis and implementation of gain-scheduling and LPV controllers for an AMB system," *Automatica*, vol. 48, no. 3, pp. 521–527, 2012.

[19] S. Zheng, Q. Chen, and H. Ren, "Active balancing control of AMB-rotor systems using a phase-shift notch filter connected in parallel mode," *IEEE Transactions on Industrial Electronics*, vol. 63, no. 6, pp. 3777–3785, 2016.

[20] Y. Okada, B. Nagai, and T. Shimane, "Cross-feedback stabilization of the digitally controlled magnetic bearing," *Journal of Vibration and Acoustics*, vol. 114, no. 1, pp. 54–59, 1992.

[21] S. Kallio, M. Andriollo, A. Tortella, and J. Karttunen, "Decoupled *d-q* model of double-star interior-permanent-magnet synchronous machines," *IEEE Transactions on Industrial Electronics*, vol. 60, no. 6, pp. 2486–2494, 2013.

[22] A. Pigazo, V. Í. M. Moreno, and E. J. EstÉbanez, "A recursive park transformation to improve the performance of synchronous reference frame controllers in shunt active power filters," *IEEE Transactions on Power Electronics*, vol. 24, no. 9, pp. 2065–2075, 2009.

[23] H. E. P. de Souza, F. Bradaschia, F. A. S. Neves, M. C. Cavalcanti, G. M. S. Azevedo, and J. P. de Arruda, "A method for extracting the fundamental-frequency positive-sequence voltage vector based on simple mathematical transformations," *IEEE Transactions on Industrial Electronics*, vol. 56, no. 5, pp. 1539–1547, 2009.

[24] J. Karttunen, S. Kallio, P. Peltoniemi, P. Silventoinen, and O. Pyrhonen, "Decoupled vector control scheme for dual three-phase permanent magnet synchronous machines," *IEEE Transactions on Industrial Electronics*, vol. 61, no. 5, pp. 2185–2196, 2014.

[25] K.-J. Lee, J.-P. Lee, D. Shin, D.-W. Yoo, and H.-J. Kim, "A novel grid synchronization PLL method based on adaptive low-pass notch filter for grid-connected PCS," *IEEE Transactions on Industrial Electronics*, vol. 61, no. 1, pp. 292–301, 2014.

[26] S. Zheng, B. Han, R. Feng, and Y. Jiang, "Vibration suppression control for AMB-supported motor driveline system using synchronous rotating frame transformation," *IEEE Transactions on Industrial Electronics*, vol. 62, no. 9, pp. 5700–5708, 2015.

[27] M. Kesler and E. Ozdemir, "Synchronous-reference-frame-based control method for UPQC under unbalanced and distorted load conditions," *IEEE Transactions on Industrial Electronics*, vol. 58, no. 9, pp. 3967–3975, 2011.

[28] M. A. Ibrahim, H. Kuntman, and O. Cicekoglu, "First-order all-pass filter canonical in the number of resistors and capacitors employing a single DDCC," *Circuits, Systems & Signal Processing*, vol. 22, no. 5, pp. 525–536, 2003.

[29] S. Minaei and O. Cicekoglu, "A resistorless realization of the first-order all-pass filter," *International Journal of Electronics*, vol. 93, no. 3, pp. 177–183, 2006.

[30] S. Maheshwari, "Voltage-mode all-pass filters including minimum component count circuits," *Active and Passive Electronic Components*, vol. 2007, pp. 1–5, 2007.